Theory and Simulation of Optical Banded Textures of Nematic Polymers during Shear Flow

W. H. Han[†] and A. D. Rey*

Department of Chemical Engineering, McGill University, 3480 University Street, Montreal, Quebec H3A 2A7, Canada

Received May 10, 1995; Revised Manuscript Received September 6, 1995[⊗]

ABSTRACT: Simulations of banded texture optical phenomena during shearing of liquid crystalline polymers are presented. A computational analysis of the polarized light transmission pattern for the nonhomogeneous orientation structure of a representative nematic polymer during shear start-up flow is presented. Simulations show that the shear-induced structure that gives rise to the banded texture is an array of tubular orientation inversion walls whose axes are normal to the flow direction. The corresponding optical computations are in good agreement with the experimentally observed banded textures of light transmission under crossed polars of sheared poly(γ-benzyl-L-glutamate) (PBLG) (Yan, N. X.; Labes, M. M. *Macromolecules* **1994**, *27*, 7843). The computer simulations show the intimate relation between the light transmission pattern and the tubular orientation inversion wall array and, hence, shed a new light on the origin of this ubiquitous phenomenon.

1. Introduction

Since the 1950s many experimental observations of light transmission patterns of sheared liquid crystalline polymers under crossed polars have reported a ubiquitous image, known as the banded texture.[1-8] Recently, a clear banded texture image during shear start-up flow of a nematic polymer has been reported, using strong homeotropic orientation anchoring conditions with a monodomain initial condition;[9] the relations between the band texture characteristics, the molecular weight, and the shear rates have also been experimentally determined. Experimental studies[2-9] have established that the banded texture is a result of some periodic spatial modulation of the orientation, leading to a spatial variation of the effective birefringence. The banded texture can be frozen-in, and correlations between the banded texture and anisotropic mechanical properties indicate the importance of a better understanding of this phenomenon.[10]

A fundamental rheological property of a nematic liquid crystal is its ability to orient close to the flow direction and in the shear plane when subjected to shear flow. Nematics displaying this property are known as flow-aligning.[11] The flow-aligning angle for uniaxial nematics is known as the Leslie angle and typically is less than 10°. Nematics that lack the ability to orient close to the shear flow direction are commonly known as nonaligning. Frequently, orientation transitions involving the loss or appearance of alignment are observed. Loss of alignment gives rise to complex orientation transient and stationary patterns.[12,13] For single component nematic liquid crystals, shear flow alignment is a rheological property that may depend on the magnitude of the shear rate[14] and temperature.[11] The shear flow-aligning properties of nematics can be identified by tracing the rotational motion of the optic axis, or the unit vector called the director (**n**), using the conoscopy method.[6] The driving forces that differentiate the rheological behavior of nematic liquid crystals are commonly identified with the viscous and elastic torques acting on the macroscopic average orientation. For aligning nematics oriented at the Leslie angle, viscous torques vanish and the resulting stationary texture is spatially uniform. On the other hand, for nonaligning nematics there is no orientation at which the viscous torques vanish, and a stationary spatially modulated three-dimensional texture is usually computed by a balance of viscous and elastic torques. The complex variety of out-of-plane textures displayed by nonaligning nematic liquid crystals subjected to start-up and steady shear flows has been elucidated in a series of recent publications.[12]

In the Leslie–Ericksen theory used in the present paper, a single temperature-dependent dimensionless coefficient, known as the reactive parameter (λ), determines whether a nematic liquid crystal subjected to shear flow is shear-aligning or not.[11] Most low molecular weight nematics are of the aligning type ($\lambda \geq 1$), while many nematic polymers are of the nonaligning type ($\lambda < 1$).[6] Since only nonaligning nematics give rise to modulations in the spatial orientation, nematic polymers showing banded textures during shear are most likely to belong to the nonaligning class.

Using the full Leslie–Ericksen equations, transient and steady state computational analyses on the flow and orientation transitions from planar to nonplanar orientation states have been carried out for both low molar mass nematics,[15] and for a nematic polymer.[16] The critical role of the nonplanar three-dimensional orientation has been demonstrated in the numerical simulations of transient and steady state rheological responses for low molar mass nematics.[17] Also, the temperature-dependent rheological responses with the underlying orientation texture have been elucidated.[18] All of the rheological computations were in very good agreement with complex experimental observations under various flow histories.[19,20] For weak flows, we thus expect that the solutions to the L-E theory will also provide a good fit to experimental data obtained using nematic polymers, well characterized boundary conditions, and monodomain initial conditions. Nonplanar orientation is an essential ingredient to the appearance of the optical banded patterns, and these periodic patterns appear to be compatible and consistent with previously obtained 1-D nonplanar textures of nonaligning nematic polymers in shear flows.[12]

[†] Present address: Polymers Division, National Institute of Standards and Technology, Gaithersburg, MD 20899.

[⊗] Abstract published in *Advance ACS Abstracts,* November 1, 1995.

0024-9297/95/2228-8401$09.00/0

Most theoretical studies on the shear-induced banded textures have been mainly concerned with the stability of weak perturbations on spatially uniform orientation states using the Leslie–Ericksen (L-E) nematodynamics equations.[21,23] Recently, we have computed the transient nonplanar (three-dimensional) orientation pattern formation during shear flow of a liquid crystalline polymer, using the full L-E equations and experimentally measured anisotropic viscoelastic material constants.[24] The computational results captured periodic pattern formation phenomena, leading to the formation of an array of tubular orientation inversion walls.[11] The periodic patterns were computed using an initially uniform orientation and a strong homeotropic surface orientation anchoring,[25] which is one of the most frequently employed experimental surface condition.[26] Here, we extend the work reported in the literature[12] and compute optical patterns arising from two-dimensional nonplanar orientation textures, and show that the light transmission computations are in good agreement with the experiments of Yan and Labes,[9] conducted with similar material and flow conditions.

The organization of this paper is as follows. Section 2 presents the L-E equations used to simulate the orientation behavior of a representative nematic polymer subjected to shear flow and defines the geometry, the governing parameters, and the boundary and initial conditions. The algorithm used to compute the light transmission from a shear flow cell is presented. Section 3 presents the results and discussion. The relation between nonplanar orientation textures and optical banded textures is elucidated, and the validation of the simulation results with the experimental data of Yan and Labes[9] is given. Finally, conclusions are given.

2. Theory and Light Transmission Simulation Method

The three-dimensional orientation structure of a nematic polymer during shear flow has been obtained by numerically solving the Leslie-Ericksen (L-E) equations, which consists of the linear momentum balance and the torque balance acting on the director.[12] The nonplanar three-dimensional orientation texture is a function of two spatial coordinates: one is the flow direction and the other is the velocity gradient direction. The linear momentum balance is given by:

$$\rho\dot{\mathbf{v}} = \mathbf{f} + \nabla\cdot\boldsymbol{\sigma} \tag{1}$$

where ρ, $\mathbf{v}$, $\mathbf{f}$, and $\boldsymbol{\sigma}$ are the density, velocity, body force per unit volume, and total stress, respectively. The superposed dot denotes the material time derivative. The total stress tensor $\boldsymbol{\sigma}$ is given by

$$\boldsymbol{\sigma} = -p\boldsymbol{\delta} - \frac{\partial F}{(\partial\nabla\mathbf{n})^{\mathrm{T}}}\cdot\nabla\mathbf{n} + \alpha_1(\mathbf{nn:A})\mathbf{nn} + \alpha_2\mathbf{nN} + \alpha_3\mathbf{nN} + \alpha_4\mathbf{A} + \alpha_5\mathbf{nn}\cdot\mathbf{A} + \alpha_6\mathbf{A}\ \text{cenn} \tag{2}$$

where p, $\boldsymbol{\delta}$, α_i (i = 1, ..., 6), $\mathbf{A}$, and $\mathbf{N}$ are the pressure, unit tensor, Leslie viscosity coefficients, rate of deformation tensor, and corotational time derivative of $\mathbf{n}$, respectively. The rate of deformation tensor $\mathbf{A}$ and the corotational time derivative of the director $\mathbf{N}$ are given by

$$2\mathbf{A} = (\nabla\mathbf{v} + (\nabla\mathbf{v})^{\mathrm{T}}) \tag{3}$$

$$\mathbf{N} = \dot{\mathbf{n}} - \boldsymbol{\omega}\cdot\mathbf{n} \tag{4}$$

where the rate of rotation tensor $\boldsymbol{\omega}$ is

$$2\boldsymbol{\omega} = (\nabla\mathbf{v} - (\nabla\mathbf{v})^{\mathrm{T}}) \tag{5}$$

The torque balance is given by

$$0 = \boldsymbol{\Gamma}^{\mathrm{v}} + \boldsymbol{\Gamma}^{\mathrm{e}} \tag{6}$$

where the viscous torque $\boldsymbol{\Gamma}^{\mathrm{v}}$ and the elastic torque $\boldsymbol{\Gamma}^{\mathrm{e}}$ are given by:

$$\boldsymbol{\Gamma}^{\mathrm{v}} = -\mathbf{n}\times(\gamma_1\mathbf{N} + \gamma_2\mathbf{A}\cdot\mathbf{n}) \tag{7}$$

$$\boldsymbol{\Gamma}^{\mathrm{e}} = -\mathbf{n}\times\left(\frac{\partial F}{\partial\mathbf{n}} - \nabla\cdot\frac{\partial F}{\partial(\nabla\mathbf{n})^{\mathrm{T}}}\right) \tag{8}$$

where γ_1 and γ_2 are the rotational and irrotational viscosities, respectively.[12] The reactive parameter λ that controls the rheological behavior of nematics is given by:

$$\lambda = -\frac{\gamma_2}{\gamma_1} \tag{9}$$

The Frank orientation curvature elastic energy F is given by:

$$2F = K_{11}(\nabla\cdot\mathbf{n})^2 + K_{22}(\mathbf{n}\cdot\nabla\times\mathbf{n})^2 + K_{33}|\mathbf{n}\times\nabla\times\mathbf{n}|^2 \tag{10}$$

where K_{11}, K_{22}, and K_{33} are the splay, twist, and bend constants, respectively. The orientation behavior during flow is controlled by the Ericksen number $\mathcal{E}$, a characteristic ratio between the viscous and elastic torques, given by

$$\mathcal{E} = \frac{\gamma_1\dot{\gamma}_2 h^2}{(\prod_{i=1}^{3}K_{ii})^{1/3}} \tag{11}$$

where $\dot{\gamma}$ and h denote the apparent shear rate and the gap thickness, respectively. The experimentally measured material constants are (γ_1, γ_2) = (6.938, −6.902) Pa·s and (K_{11}, K_{22}, K_{33}) = (1.21, 0.078, 0.763) × 10^{-11} N.[24] Note that the Ericksen number is proportional to $\dot{\gamma}$.

To investigate the optical responses of nonhomogeneous nonplanar three-dimensional orientation during shear flow of polymeric nematics, this work performs a computation of the polarized light transmission intensity pattern using the previously computed nonhomogeneous three-dimensional orientation field $(n_x(x,y,\gamma), n_y(x,y,\gamma), n_z(x,y,\gamma))$,[25] where γ denotes the applied shear strain, x the flow direction, y the velocity gradient direction, and z the vorticity direction. The effect of the spatial orientation variation $(n_x(x,y,\gamma), n_y(x,y,\gamma), n_z(x,y,\gamma))$ along the flow (x) direction as well as the thickness (y) direction (light propagation direction) on the light transmission intensity pattern has been taken into account. When the orientation is uniform along the light propagation direction (y-axis), as shown in Figure 1(a), the computation of light transmission through a nematic sample is the same as that for a uniaxial single crystal, while when the orientation variation occurs along the light propagation direction, as shown in Figure 1(b), a more elaborate method to compute light

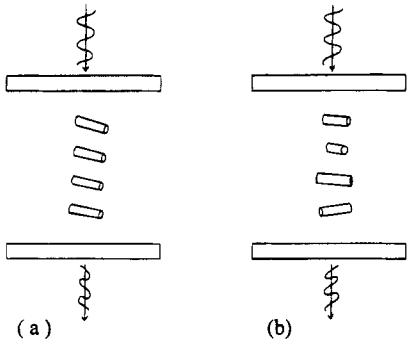

Figure 1. Electromagnetic wave (light) propagation through anisotropic media. (a) Homogeneous orientation and (b) nonhomogeneous orientation along the light propagation direction.

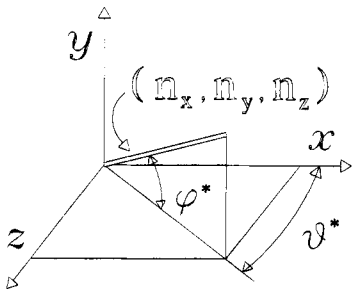

Figure 2. Relation between the director angles (ϕ^*, θ^*) and the Cartesian coordinate system of the shear flow geometry. Flow direction: x; velocity gradient direction: y; vorticity direction: z. When $\theta^* = 0$ ($\theta^* \neq 0$), the orientation is planar (nonplanar).

transmission to take into account the corresponding variation of the anisotropic refractive indices is required.[27] In the present light transmission simulation, light with normal incidence first goes through the polarizer parallel to the flow direction (x-axis), then through the nematic polymer sample of spatially nonhomogeneous orientation, and finally through the analyzer that is orthogonal to the polarizer. To compute the light transmission, a standard method for uniaxial crystals has been used.[28,29]

The sample is discretized into a series of different homogeneous thin orientation layers normal to the light propagation direction (y-axis), with a thickness comparable to one wavelength of a given monochromatic light. For each homogeneous orientation layer, the amplitudes and orientations of the ordinary and extraordinary light vibration vector for a given three-dimensional orientation, as well as the phase lag between the ordinary and extraordinary light rays, are computed. Figure 2 shows the relation between the director orientation angles and the Cartesian coordinate system of the shear flow geometry used for the computation of the light transmission. The relations between the director components and the spherical angles are given by:

$$n_x = \cos\phi^* \cos\theta^*, \quad n_y = \sin\phi^*, n_z = \cos\phi^* \sin\theta^* \tag{12}$$

Here, the x-axis and z-axis are parallel to the polarizer and analyzer, respectively. In the light transmission simulation, we assume normal incidence and nonabsorbing rectilinear light propagation through a uniaxial nematic polymer. Let us consider layer 1, say, of orientation (ϕ^*_1, θ^*_1), and the adjacent layer 2 of orientation (ϕ^*_2, θ^*_2), along the light propagation direction. We now use complex variable representation for the ordinary and extraordinary rays to take into account the polarization and the phase lag. The complex amplitudes of light along the ordinary and extraordinary vibration directions for the light emerging from layer 1 are denoted by A_{o1} and A_{e1}, respectively. After passing through layer 2, the emerging light has complex amplitudes (A_{o2}, A_{e2}) that are given by:[28]

$$A_{o2} = A_{e1} \sin(\theta^*_2 - \theta^*_1) + A_{o1} \cos(\theta^*_2 - \theta^*_1),$$

$$A_{e2} = (A_{e1} \cos(\theta^*_2 - \theta^*_1) - A_{o1} \sin(\theta^*_2 - \theta^*_1)) \times \exp(-i\delta) \tag{13}$$

where the phase lag δ is a function of the birefringence ($n_e - n_o$), the light wavelength λ_e, the orientation layer thickness h_l, and the orientation angle ϕ^*_2, as follows:

$$\delta = 2\pi(n_e - n_o)h_l (\cos^2 \phi^*_2)/\lambda_e \tag{14}$$

which is equivalent to eq 36 of the monograph,[28] noting that the relation between ϕ^*_2 in the present manuscript and θ in eq 36 of the monograph[28] is $\phi^*_2 = \pi/2 - \theta$ for normal incident light.

This procedure is repeated through all orientation layers.[29] Since the polarizer is parallel to the flow direction, the effect of the presence of the polarizer just before the nematic polymer sample is taken into account by assuming the polarizer as layer 1 in the following equation for the complex amplitudes:

$$A_{o1} = \sin\theta^*_1 \exp(i\omega t)$$

$$A_{e1} = \cos\theta^*_1 \exp(i\omega t) \exp(-i\delta) \tag{15}$$

which is used in the initial step in the computational light transmission scheme mentioned above. The presence of the analyzer (parallel to z-axis) adjacent to the final orientation layer n in the light propagation path is taken into account by the following equation for light transmission intensity I:

$$I = \langle (A_{en} \sin\theta^*_n - A_{on} \cos\theta^*_n) \times \overline{(A_{en} \sin\theta^*_n - A_{on} \cos\theta^*_n)} \rangle \tag{16}$$

where the overbar denotes a conjugate complex number. To simulate the experimental observations,[9] we use a sample thickness value of 20 μm and a monochromatic light wavelength of 632.8 nm (He-Ne laser light wavelength). The refractive indices for the ordinary ray (n_o) and for the extraordinary rays (n_e) for the well-known LCP [poly(γ-benzyl glutamate)] used in this study are as follows: $n_o = 1.450$, $n_e = 1.456$.[26] Next, we show representative light transmission simulations results that best meet the objective of this paper.

3. Results and Discussion

Figure 3 shows three-dimensional plots for the director components of the director field (n_x, n_y, n_z) for a shear strain of $\gamma = 239.77$ and strong homeotropic anchoring conditions ($n_y = 1$ at $y = 0$, h). A large (1:16) thickness to length ratio of the computational domain is used to simulate a more realistic system. The plot of the n_x component shows a continuous planar orientation matrix ($n_x \approx +1$) with about nine collapsed plateau regions representing an antiparallel planar orientation matrix ($n_x \approx -1$). The plot of the n_y component shows a relatively small variation around $n_y = 0$, indicating that

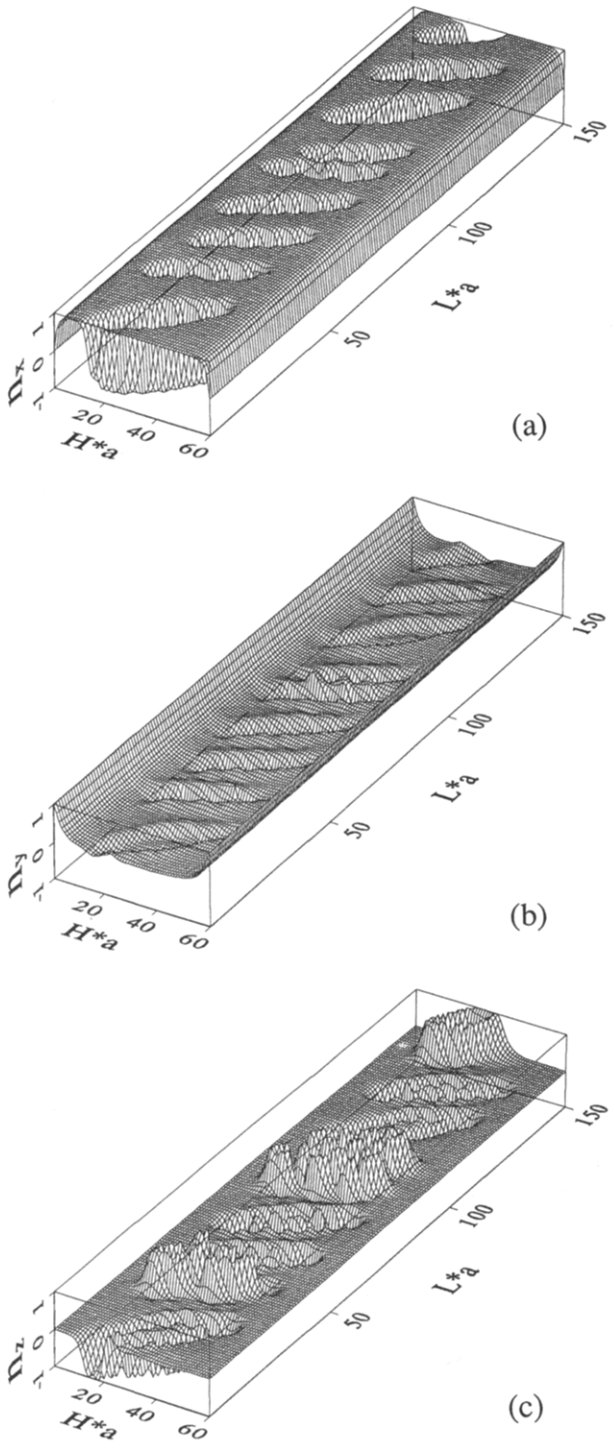

Figure 3. Surface plots of the 3-D director components (n_x, n_y, n_z) as a function of x (flow direction) and y (velocity gradient direction), for a shear strain of $\gamma = 239.77$, and homeotropic surface orientation anchoring. The axes scale factors for the dimensionless height ($H = y/h$) and length ($L = x/h$) are (a, b) = (60, 9.375). The Ericksen number ($\mathcal{E}$) is 2918.

the orientation is mainly associated with distortions within the $x-z$ plane. Therefore, the n_x or n_z component can show the main characteristics of the orientation texture. The n_z component plot shows regions with locally concentrated nonplanar orientation, known as inversion walls.[30]

Figure 4(a) shows a scientific visualization of the out-of-shear plane component (n_z) (shown in Figure 3); the gray scale corresponds to the magnitude and sign of n_z: $n_z > 0$ and a large magnitude correspond to light regions, $n_z < 0$ and a large magnitude correspond to

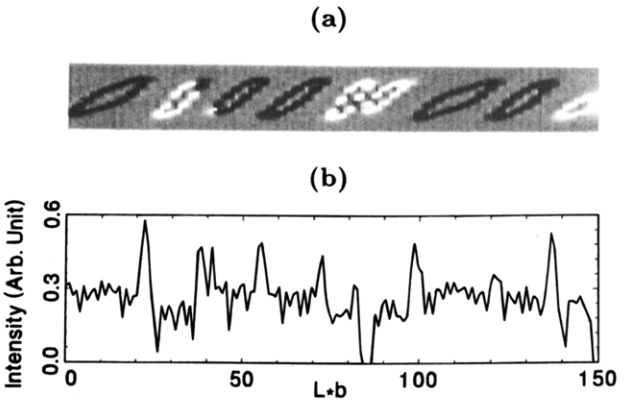

Figure 4. (a) Scientific visualization of the n_z director component shown in Figure 2. The long and short axes of the plot represent the flow and thickness directions, respectively. Dark and bright stripes represent $n_x \approx -1$ and $n_z \approx +1$ director orientations (orientation inversion walls), respectively, and a mid-gray area represents a planar orientation matrix ($n_z \approx 0$). The Ericksen number ($\mathcal{E}$) is 2918, and the applied shear strain (γ) is 239.77. (b) Light transmission intensity as a function of dimensionless length (Lb) corresponding to the director field shown in Figure 3. The scale factor b is 9.375, the same as in Figure 3.

dark regions, and $n_z \approx 0$ (planar orientation) is shown as gray. The figure clearly shows the presence of an array of tubular orientation inversion walls[30] immersed in a matrix of planar ($n_z \approx 0$) orientation, whose axes are orthogonal to the flow (x) direction. As mentioned above, dark and bright stripes represent $n_z \approx 1$ and $n_z \approx +1$ director orientations (orientation inversion walls), respectively, while a medium gray area represents a planar orientation matrix ($n_z \approx 0$). The tubular orientation inversion walls divide the continuous planar orientation matrix ($n_x \approx +1$), lying outside the inversion walls, from the dispersed planar orientation matrices ($n_x \approx -1$) lying inside the tubular inversion walls.

Figure 4(b) shows the light transmission intensity as a function of dimensionless length (L) along the x-axis under crossed polars, for the corresponding three-dimensional orientation structure shown in Figures 3 and 4.

According to the experimental observations,[9] as the shear rate increases, the wavelength decreases from infinity to a saturation value equal to the half-gap thickness. At intermediate shear rates, the wavelength of the banded texture is of the order of the gap thickness (h). The infinite wavelength occurs at a critical shear rate, or equivalently at critical Ericksen number $\mathcal{E}_c$, corresponding to the planar–nonplanar orientation transition.[16] The critical Ericksen number $\mathcal{E}_c$ for periodic pattern formation is found to be very close to the critical Ericksen number for the nonperiodic planar–nonplanar orientation transition.[16] The transition from nonplanar nonperiodic textures to nonplanar periodic textures that appears when shearing a nematic polymer at sufficiently high shear rates arises from the coupling between competing elastic and viscous effects. Elastic effects favor a nonperiodic nonplanar texture since they contain less elastic distortion, while viscous effects favor the formation of a periodic nonplanar texture since the associated governing Miesowicz viscosities[11] are relatively lower.[25]

Figure 4(b) shows that there are about 8 major peaks in the light transmission distribution, which means that the wavelength of the banded texture for the shown Ericksen number is $O(h)$, where h is the gap thickness, which is in good agreement with experiments.[9] As

mentioned above, Yan and Labes[9] show that as the Ericksen number increases, the band wavelength saturates to a value equal to half the gap thickness. Since the present study considers the shear flow for an Ericksen number not much larger than the critical Ericksen number $\mathcal{C}_c$ for nonplanar periodic texture formation ($\mathcal{C}_c \approx 2600$),[16] the computed wavelength is larger than the saturation value that would be observed at much higher Ericksen numbers.

Panels (a) and (b) of Figure 4 show that the transmission intensity maxima occur between two adjacent tubular orientation inversion walls. Each of the elongated and tilted tubular orientation structures (see dark and light ellipses in Figure 4(a)) that forms part of the tubulary array gives rise to a lower light transmission in the central part of the structure, and a higher transmission around the tip of the structure. When two adjacent orientation tube structures strongly overlap each other, the light transmission is very low, while if the overlap between two tubular structures is weak, the light transmission is a maximum. Thus, the relative difference between the transmission intensity peaks are due to different orientation distortion mediation modes associated with pairs of adjacent tubular orientation inversion walls. For example, starting from the left, the first peak is taller than the rest of the peaks since for the first peak there is overlapping between adjacent tubular orientation inversion walls. Also, note that the maximum overlapping between adjacent tubular inversion walls, shown in the middle of Figure 4(a), results in the lowest light transmission.

4. Conclusions

Summarizing, we computed the light transmission intensity of a nonaligning nematic polymer in shear start-up flow that shows banded textures, in agreement with those observed in the experiments of Yan and Labes.[9] The orientation structure that gives rise to the optical banded texture has been shown to have an orientation variation in the light propagation direction in addition to the spatial orientation variation normal to the bands. The results of the simulations provide new insights on the correlation between textures and optical transmission patterns. These nontrivial correlations suggest the need for additional measurements on the optical banded textures of nematic polymers in shear start-up flows.

Acknowledgment. This work was supported by a research grant from Natural Science and Engineering Research Council of Canada.

References and Notes

(1) Elliott, A.; Ambrose, E. J. *Discuss. Faraday Soc.* **1950**, *9*, 246.
(2) Toth, W. J.; Tobolsky, A. V. *Polym. Lett.* **1970**, *8*, 537.
(3) Kiss, G.; Porter, R. S. *Mol. Cryst. Liq. Cryst.* **1980**, *60*, 267.
(4) Donald, A. M.; Viney, C.; Windle, A. H. *Polymer* **1983**, *24*, 155.
(5) Navard, P. J. *Polym. Sci.: Phys. Ed.* **1986**, *24*, 435.
(6) Srinivasarao, M.; Berry, G. C. *J. Rheol.* **1991**, *35*, 379.
(7) Larson, R. G.; Mead, D. W. *Liq. Cryst.* **1992**, *12*, 751.
(8) Vermant, J.; Moldenaers, P.; Picken, S. J.; Mewis, J. *J. Non-Newtonian Fluid Mech.* **1994**, *53*, 1.
(9) Yan, N. X.; Labes, M. M. *Macromolecules* **1994**, *27*, 7843.
(10) Wang, J.; Labes, M. M. *Macromolecules* **1992**, *25*, 5790.
(11) de Gennes, P. G.; Prost, J. *The Physics of Liquid Crystals*; Clarendon Press: Oxford, 1993; Chapter 5.
(12) Han, W. H.; Rey, A. D. *Phys. Rev. E* **1994**, *49*, 597.
(13) Han, W. H.; Rey, A. D. *Phys. Rev. E* **1994**, *50*, 1688.
(14) Marrucci, G. In *Liquid Crystallinity in Polymers*; Ciferri, A., Ed.; VCH: New York, 1991; Chapter 11.
(15) Han, W. H.; Rey, A. D. *J. Non-Newtonian Fluid Mech.* **1993**, *48*, 181.
(16) Han, W. H.; Rey, A. D. *J. Non-Newtonian Fluid Mech.* **1993**, *50*, 1.
(17) Han, W. H.; Rey, A. D. *J. Rheol.* **1994**, *38*, 1317.
(18) Han, W. H.; Rey, A. D. *J. Rheol.* **1994**, *39*, 301.
(19) Gu, D.; Jamieson, A. M.; Wang, S. *J. Rheol.* **1993**, *37*, 985.
(20) Gu, D.; Jamieson, A. M. *J. Rheol.* **1994**, *38*, 555.
(21) Manneville, P.; Dubois-Violette, E. *J. Phys.* **1976**, *37*, 285.
(22) Zielinska, B. J. A.; Ten Bosch, A. *Phys. Rev. A* **1989**, *38*, 5465.
(23) Larson, R. G. *J. Rheol.* **1993**, *37*, 175.
(24) Srajer, G.; Fraden, S.; Meyer, R. B. *Phys. Rev. A* **1989**, *39*, 4828.
(25) Han, W. H.; Rey, A. D., submitted for publication in *Phys. Rev. Lett.*, 1995.
(26) Dupré, D. B. In *Polymer Liquid Crystals*; Ciferri, A., Krigbaum, W. R., Meyer, R. B., Eds.; Academic Press: New York, 1982; Chapter 7.
(27) Viney, C. In *Liquid Crystalline Polymers*; Weiss, R. A., Ober, C. K., Eds.; American Chemical Society: Washington, DC, 1990.
(28) Born, M.; Wolf, E. *Principles of Optics*, 6th ed.; Pergamon Press: Oxford, 1980; pp 695 and 699.
(29) Nicholson, T. M. *Mol. Cryst. Liq. Cryst.* **1989**, *177*, 163.
(30) Rey, A. D. *Liq. Cryst.* **1990**, *7*, 315.

MA950632J